ISSN 0967-0912, Steel in Translation, 2021, Vol. 51, No. 12, pp. 859–865. © Allerton Press, Inc., 2021.
Russian Text © The Author(s), 2021, published in Izvestiya Vysshikh Uchebnykh Zavedenii, Chernaya Metallurgiya, 2021, No. 12, pp. 886–894.

# Physical Nature of Rail Surface Hardening during Long-Term Operation

**B. P. Yur'ev[a, *], V. E. Kormyshev[b, **], V. E. Gromov[b, ***], Yu. F. Ivanov[c, ****], and Yu. A. Shlyarova[b, *****]**

[a] *JSC EVRAZ—Joint West Siberian Metallurgical Plant, Novokuznetsk, 654043 Russia*
[b] *Siberian State Industrial University, Novokuznetsk, 654007 Russia*
[c] *Institute of High-Current Electronics, Siberian Branch of the Russian Academy of Sciences, Tomsk, 634055 Russia*
**e-mail: ant-yurev@yandex.ru*
***e-mail: 89236230000@mail.ru*
****e-mail: gromov@physics.sibsiu.ru*
*****e-mail: yufi55@mail.ru*
******e-mail: rubannikova96@mail.ru*

Received June 16, 2020; revised June 29, 2020; accepted October 11, 2021

**Abstract**—A comparative quantitative analysis of the physical mechanisms of hardening of rail surface layers after extremely long-term operation is performed. The method is based on the previously established regularities in the formation of structural-phase states and mechanical properties of differentially hardened long-length rails produced by JSC EVRAZ ZSMK at a depth of up to 10 mm in the rail head along the central axis and fillet after the passed tonnage of 1411 million tons. The calculations consider the volume fractions and characteristics of particular substructure types. The increase in the microhardness and hardness of the surface layers of the rails exposed to extremely operation on the experimental ring of the Russian Railways is multifactorial and determined by the superposition of a number of physical mechanisms. The contributions conditioned by the friction of the matrix lattice, intraphase boundaries, dislocation substructure, presence of carbide particles, internal stress fields, solid hardening, and pearlitic component of the steel structure are estimated. The strength of the rail metal depends on the distance to the surface: it increases on approaching the top of the head and does not depend on the analysis direction (along the central axis of the head or along the fillet symmetry axis). The most significant physical mechanisms are established, which ensure high strength properties of the metal of the rail head exposed to extremely long-term operation. In the subsurface layer of the rail head at a depth of 2–10 mm, the most significant physical mechanism is dislocation conditioned by the interaction of moving and stationary dislocations (*forest* dislocations). In the surface layer of the rail head, the most significant physical mechanism is substructural conditioned by the interaction of dislocations with small-angle boundaries of fragments and subgrains of nanometer polygons. A comparison with the quantitative values of the rail hardening mechanisms after the passed tonnage of 691.8 million tons is performed. It is shown that an increase in the passed tonnage in the range of 691.8–1411 million tons significantly increases the steel strength by 50 or 100%.

**Keywords:** rails, surface layers, hardening mechanisms, long-term operation, structure, phase composition, rolling surface, fillet

**DOI:** 10.3103/S0967091221120147

## INTRODUCTION

The formation and evolution of structural phase states and properties of rail surface layers during long-term operation are a complex set of interrelated research and engineering issues. In this domain, the importance of information is determined by the profundity of understanding the basic issues of condensed-state physics, on the one hand, and by the practical significance of the problem, on the other [1].

Rail hardening and wear issues have received a detailed coverage in Russian and foreign research works published in recent years. It has been proven that wear defects initially form in surface layers in which case the beginning of wear coincides with the accumulation of a certain level of plastic strains [2–8].

High values of rail performance characteristics must be formed on the basis of knowing the mechanisms of structural phase changes along the section of rails exposed to long-term operation. These mechanisms are detected only by analyzing regularities in the evolution of fine structural parameters and estimating the contribution of structural constituents and defec-

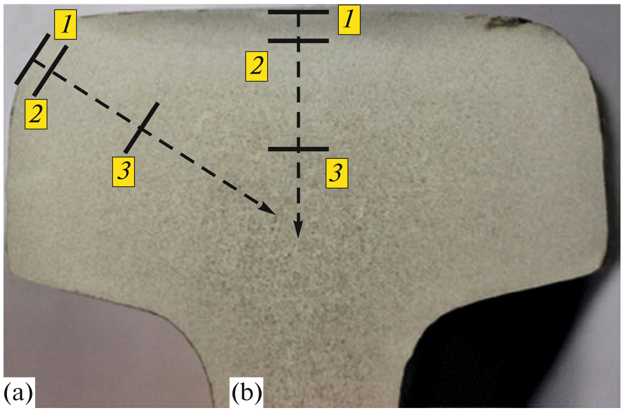


**Fig. 1.** Diagram of the specimens test along the fillet (a) and along the central axis (b): (*1*) is the rail head running; (*2*) and (*3*) is the layer at distances of 2 and 10 mm from the surface.

tive substructure in the hardening of rails during long-term operation.

At modern railroad train speeds and high contact pressures, relatively low passed tonnage causes cementite decomposition, abnormally high microhardness, and significant structural changes in the rail surface. The rails exposed to long-term operation accumulate multiple defects, which can be attended by the downgrading of their physical and mechanical properties and make the rails break.

The physical nature of the surface layers of rails differentially quenched along the central axis and the fillet after passing the tonnage of 691.8 million tons was identified in the works generalized in monograph [9] on the basis of the integral quantitative studies of the structure, phase composition, defect substructure, and mechanical properties of rails. The contributions to the hardening of volumetrically quenched rails after the passed tonnage of 500 and 1000 million tons were identified in studies [1, 10].

This work is intended to evaluate the mechanisms and identify the physical nature of the hardening of the surface of 100-m rails differentially quenched along the central axis and the fillet after extremely long-term operation on a test ring of the Russian Railways.

## MATERIALS AND METHODS

The specimens chosen for the study were differentially quenched DT350 rails removed from the tracks of the test ring of the Russian railways after the gross passed tonnage of 1411 million tons.

Integral quantitative studies of the structure, phase composition, defect substructure, and tribological properties at various distances from the rail head running surface along the central axis and the fillet were conducted by modern physical material science methods, such as optical, scanning, and transmission microscopy, hardness and tribological measurements, X-ray structural analysis [11–15]. For the specimen test layout, see Fig. 1.

## RESULTS AND DISCUSSION

The hardness along the head section was transversely measured in studies [11–15]. It has been established that the respective *HRC* hardness at a depth of 2, 10, 22 mm is 37.1, 35.8, and 35.6. The microhardness at a depth of 2 mm is 1481 mPa, whereas at a depth of 10 mm the microhardness is much lower and reaches 1210 mPa. This difference in the microhardness by thickness is clearly conditioned by the structural phase changes in the metal of the rails in use. The results of analyzing the structure and phase composition of the steel are presented in works [11–15] and attest the multifactorial hardening of the material. The obtained quantitative characteristics of the steel structure allow considering the physical nature of the increase in the strength of steel, evaluating its hardening mechanisms, and identifying the dominant mechanisms that determine its strength. Since the morphological and phase diversity of the structure of steel could not be considered in determining the microhardness of the material, the quantitative estimation of the steel hardening mechanisms was performed by the quantitative characteristics averaged for the volume of the material, considering the volumetric fraction and characteristics of a particular type of substructure.

The hardening mechanism values were estimated using broadly used expressions [16–39].

The rail hardening conditioned by lamellar perlite can be evaluated according to the following expression from [16, 17]:

$$\sigma(\mathrm{P}) = k_y(4.75L)^{-1/2}0.24V(\mathrm{P}),$$

where $L$ is the distance between the cementite plates; $V$(P) is the relative content of lamellar perlite in steel; $k_y = 2 \times 10^{-2}$ Pa m$^{1/2}$.

The stress necessary for maintaining plastic strain, that is, creep stress $\sigma$ necessary for moving dislocations to overcome the forces of interaction with stationary dislocations (*forest* dislocations) is related to the scalar density of dislocations via the following formula from [16–23]:

$$\sigma_d = \sigma_0 + \alpha m G b\sqrt{\langle\rho\rangle},$$

where $\sigma_0$ is the nondislocation flow stress (conditioned by hardening mechanisms other than dislocation);

$\langle\rho\rangle$ is the average (scalar density) of dislocations;

$m$ is Schmidt's orientation factor;

$\alpha$ = 0.10–0.51 is the parameter characterizing the level of interdislocation interactions [24, 25];

$G$ is the steel elasticity modulus (≈80 gPa);

$b$ is Burger's dislocation vector (0.25 nm).

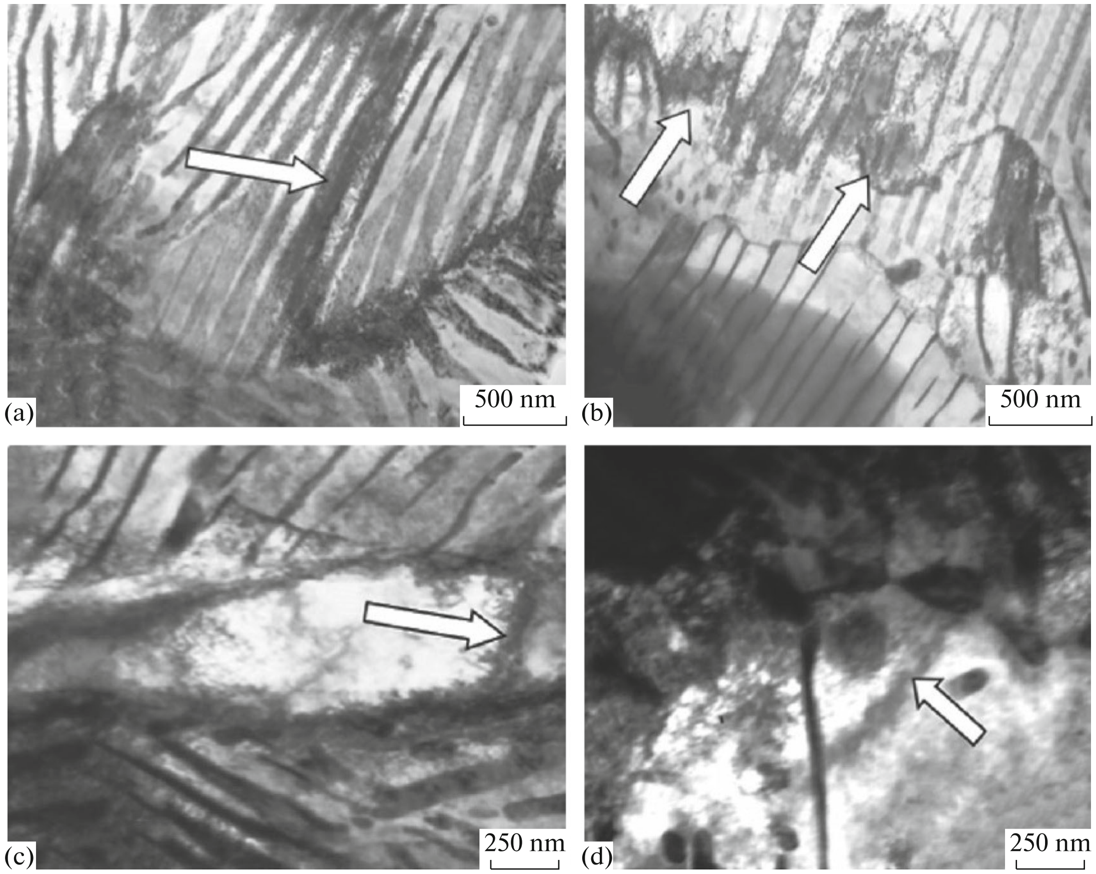


**Fig. 2.** TEM images of the rails structure (the arrows indicate the extinction contours).

Considering multiplier factor $m$, it is commonly taken for steels that $m\alpha \approx 0.5$.

The operation of rails is attended by the formation of internal stress fields in steel. When steel is examined by TEM, the presence of stress fields in the material usually shows in electron microscopic images of bended extinction contours which indicate the curvature-buckling of the crystalline lattice of a particular section of foil [1, 9].

The analysis of bended extinction contours allows identifying sources of internal stresses and their relative value, that is, detecting stress concentrators. As established by the studies, the sources of internal stress fields are interfaces of perlite grains (Figs. 2a and 2b) and perlite and ferrite grains (Fig. 2c). In this case, the contour begins from the grain boundary. Stress fields are also generated fairly frequently by secondary-phase particles located along the grain boundary and in the grain volume (Fig. 2d).

The size of plastic component σ(pl) and elastic component σ(el) of internal stress fields can be evaluated proceeding from the following ratios from [1, 9, 26]:

$$\sigma(\mathrm{pl}) = m\alpha G b\sqrt{\rho_{\pm}};$$

$$\sigma(\mathrm{el}) = m\alpha G b\chi_{\mathrm{el}},$$

where $t$ is the foil thickness (taken as 200 nm for the calculations); $\chi_{\mathrm{el}}$ is the elastic component of the curvature-buckling of the crystalline lattice.

Redundant dislocation density $\rho_{\pm}$ is related to crystalline lattice curvature-buckling gradient $\chi$ via Burger's dislocation vector $b$.

The operation of rails is attended by the dynamic aging of steel, which results in the formation of nanosize ferrous carbide particles in the material. Ferrous carbide particles bigger than 5 nm lose coherent connection with the α phase crystalline lattice [16, 27–32]. Therefore, the carbide-phase particles above 10 nm in size which are present in the rail steel are noncoherent. Noncoherent cementite particles are an obstacle to the movement of dislocations, which hardens the material. The steel hardening estimation is made considering the presence of noncoherent secondary-phase particles and using the following equation from [33]:

$$\sigma_{\mathrm{p}} = M\frac{mG_m b}{2\pi(|\lambda - D|)}\Phi\ln\left(\left|\frac{\lambda - D}{4b}\right|\right),$$

where $\lambda$ is the average interparticle distance; $D$ is the average particle size; $m$ is the orientation multiplier (for materials VCCL of 2.75); $\Phi = 1$ and $(1 - \nu)^{-1}$ for the screw and the edge dislocation, respectively; $M =$

**Table 1.** Estimates of the hardening mechanism of the rails metal after the passed tonnage of 1411 million tons

| Parameter | Value at a distance from surface, mm | | | | | |
|---|---|---|---|---|---|---|
| | 10 | 2 | 0 | 10 | 2 | 0 |
| | Rail head running surface | | | Working fillet | | |
| $\Delta\sigma$(PRL), MPa | 142.5 | 161.5 | 85.5 | 152.0 | 152.0 | 95.0 |
| $\Delta\sigma(L)$, MPa | 0 | 0 | 473.3 | 0 | 0 | 1455.6 |
| $\Delta\sigma(\rho)$, MPa | 152.8 | 181.0 | 181.4 | 164.0 | 206.0 | 190.4 |
| $\Delta\sigma(h)$, MPa | 131.3 | 149.0 | 255.0 | 148.6 | 149.6 | 230.4 |
| $\Delta\sigma$(pt), MPa | 154.1 | 148.5 | 107.0 | 80.6 | 222.9 | 195.0 |
| $\Delta\sigma$(hrd), MPa | 11.0 | 11.0 | 11.7 | 11.0 | 11.0 | 11.7 |
| $\sigma = \sum_{i=1}^{n} \sigma_i$, MPa | 591.7 | 651.0 | 1114.0 | 556.2 | 741.5 | 2178.1 |

0.81–0.85 is the parameter considering the inequal particle distribution in the matrix [25].

The operation of rails is attended by the formation of a fragmented substructure in the surface layer. The hardening of the material by low-angle boundaries (substructural hardening, hardening by fragment boundaries) dividing the fragments is estimated using the following expression from [1, 16, 22]:

$$\Delta\sigma(L) = \sigma_0 + k^* L^{-m},$$

where $m = 1$ or 1/2; $L$ is the average size of the fragments.

As established in works [16, 22, 32, 34], at $m = 1$ $k^*$ ranges from 150 to 100 N/M; at $m = 1/2$ $k^*$ ranges from $2 \times 10^{-3}$ to $10^{-2}$ Pa m$^{1/2}$.

In the calculations, it was taken that $k^* = 150$, $m = 1$.

Quantity $\sigma_0$ is the friction stress in the material's crystalline lattice, that is, the stress necessary for the movement of dislocations in single-phase pure monocrystals (w/o impurities). Stress $\sigma_0$ considerably depends on the pureness and imperfection of the material. In theoretically pure materials, this stress is 17 mPa. The test values of $\sigma_0$ range from 27 to 60 mPa [16, 24]. In steels, this stress usually ranges from 30 to 40 mPa [16].

As shown above, the operation of rails is usually attended by the dissolution (destruction) of cementite. The carbon released in this process participates in the formation of nanoparticles of secondary cementite, settles down on structural defects, and falls into interstices in the crystalline lattice of steel. The solid-solution steel hardening conditioned by carbon atoms was estimated by the following empirical expression from [16, 22, and 34–37]

$$\sigma(\text{sol}) = \sum_{i=1}^{m} (k_i C_i),$$

where $k_i$ is the ferrite hardening coefficient expressed in the change in hardness at the dissolution of 1% (weight) of an alloying element in ferrite; $C_i$ is the concentration of the element dissolved in ferrite, % (weight).

According to work [38], the value of $k_i$ for different elements is determined empirically.

The overall creep limit of steel for the first approximation based on the additivity principle is represented as a linear sum of contributions of particular hardening mechanisms [1, 9, 16, 17, 34, 39]:

$$\sigma = \Delta\sigma_0 + \Delta\sigma(\rho) + \Delta\rho(h) + \Delta\sigma(\text{pt}) + \Delta\sigma(\text{hrd}) + \Delta\sigma(\text{PRL}),$$

where $\Delta\sigma_0 = 30$ mPa is the contribution conditioned by the matrix lattice friction [16]; $\Delta\sigma(L)$ is the contribution conditioned by intraphase boundaries; $\Delta\sigma(\rho)$ is the contribution conditioned by dislocation substructure; $\Delta\sigma$(pt) is the contribution conditioned by the presence of carbide-phase particles; $\Delta\sigma(h)$ is the contribution conditioned by the internal stress fields; $\Delta\sigma$(hrd) is the contribution conditioned by solid-solution hardening; $\Delta\sigma$(PRL) is the contribution conditioned by the perlite component of the steel structure.

The additivity principle implies that the action of each of the hardening mechanisms is independent.

Thus, the determination of the quantitative characteristics of the steel structure allows analyzing, for the first approximation, the physical mechanisms responsible for the evolution of the hardness of steel during the operation of the rails as well as identifying the physical mechanisms of the formation of rail steel hardness gradient.

The steel hardening mechanisms were estimated using the results of the qualitative analysis of steel from works [11–15]. For the estimation results, see Table 1.

There are several things to note. First of all, the strength of steel is a multifactorial characteristic and

**Table 2.** Estimates of the hardening mechanism of the rails structure after passing the gross tonnage of 691.8 million tons

| Parameter | Value at a distance from surface, mm | | | | | |
|---|---|---|---|---|---|---|
| | 10 | 2 | 0 | 10 | 2 | 0 |
| | Rail head running surface | | | Working fillet | | |
| $\Delta\sigma$(PRL), MPa | 165 | 140 | 41 | 165 | 115 | 48 |
| $\Delta\sigma(L)$, MPa | 0 | 0 | 0 | 0 | 0 | 0 |
| $\Delta\sigma(\rho)$, MPa | 340 | 356 | 363 | 330 | 350 | 375 |
| $\Delta\sigma(h)$, MPa | 274 | 351 | 356 | 230 | 300 | 320 |
| $\Delta\sigma$(pt), MPa | 0 | 0 | 113 | 0 | 0 | 67 |
| $\Delta\sigma$(hrd), MPa | 0 | 0 | 133 | 0 | 0 | 133 |
| $\sigma = \sum_{i=1}^{n} \sigma_i$, MPa | 779 | 847 | 1006 | 725 | 765 | 943 |

determined by the aggregate influence of a number of physical mechanisms. Secondly, the strength of the rail metal depends on the distance to the head surface, whatever is the analyzed location (along the central axis or along the fillet symmetry axis), which agrees with the results of determining the microhardness of steel. Thirdly, the strength of the rail metal increases upon approaching the head surface. Fourthly, the main rail metal hardening mechanism in the subsurface layer of the head (at a depth of 2–10 mm) is the dislocation conditioned by the interaction of mobile and stationary dislocations (*forest* dislocations). Fifthly, the main metal hardening mechanism in the surface layer of the rail head is the substructural mechanism conditioned by the interaction of dislocations with low-angle fragment boundaries and nanometer subgrains. Another missed hardening factor that should be considered in analyzing the results is the presence of carbon atoms in crystal defects (dislocations and grain and subgrain boundaries).

In work [9], this possibility is indicated by the estimates of the structural distribution of carbon atoms in steel. The formation of atmospheres and segregations of carbon atoms on crystalline morphological flaws of steel will obviously affect their mobility, that is, strengthen the material.

The earlier estimates of the rail hardening mechanisms after the passed tonnage of 691.8 million tons [9] (Table 2) allow tracking the evolution of the aggregate creep limit in the course of operation. It is seen that an increase in the passed tonnage from 691.8 to 1411 million tons during operation significantly increases the aggregate creep limit (by 50 or 100%). In this case, the hardening process covers only the surface metal layer of no more than 2 mm in thickness.

## CONCLUSIONS

The mechanisms of the hardening of the rail head metal after the passed tonnage of 1 411 million tons have been analyzed along the fillet symmetry axis and the central axis (rail head running surface). It is shown that, in both cases, the hardening is multifactorial and determined by the superposition of several physical mechanisms.

The increase in the microhardness and hardness of the rail steel exposed to long-term operation is multifactorial and conditioned, first of all, by the substructural hardening caused by the formation of nanosize fragments with boundaries stabilized by carbide-phase particles. Secondly, this increase is conditioned by the hardening by nanosize carbide-phase particles within the fragments and dislocations (dispersion hardening). Thirdly, this increase in conditioned by the internal stress fields shaped by the strain incompatibility of adjacent grains, crystallites of various phases, and microcracks.

The most significant physical mechanisms to ensure the high strength of the metal in the head of the rails exposed to extremely long-term operation are the dislocation in the subsurface layer of the rail head (at a depth of 2 to 10 mm) and the substructural mechanism in the surface layer of the rail head. The former mechanism is conditioned by the interaction of mobile and stationary dislocations. The latter mechanism is conditioned by the interaction of dislocations with low-angle boundaries of fragments and nanometer subgrains.

The hardening mechanisms of rails operated for different periods have been compared. The increase in the tonnage from 691.8 to 1411 million tons leads to a nearly twofold increase in the aggregate creep limit. In this case, the surface layer of fillet metal is nearly two times as strong as the rail head running surface

## ACKNOWLEDGMENTS

We thank N.A. Popova for her help in the quantitative calculations of hardening mechanisms.

## FUNDING

The analysis of the structural and phase state of steel was supported by the Russian Foundation for Basic Research, project no. 19-32-60001. The analysis of the hardening mechanisms was supported by the Russian Science Foundation, project no. 19-19-00183.

## ADDITIONAL INFORMATION

**Authors ORCID ID.** A.A. Yur'ev (0000-0003-4403-9006), V.E. Kormyshev (0000-0002-5147-5343), V.E. Gromov (0000-0002-5147-5343), Y.F. Ivanov (0000-0001-8022-7958), Y.A. Shlyarova (0000-0001-5677-1427).

## REFERENCES

1. Gromov, V.E., Peregudov, O.A., Ivanov, Yu.F., Konovalov, S.V., and Yur'ev, A.A., *Evolyutsiya strukturno-fazovykh sostoyanii metalla rel'sov pri dlitel'noi ekspluatatsii* (Evolution of Structural-Phase States of Metal Rails during Long-Term Operation), Novosibirsk: Sib. Otd., Ross. Akad. Nauk, 2017.
2. Ivanisenko, Yu. and Fecht, H.J., Microstructure modification in the surface layers of railway rails and wheels, *Steel Tech.*, 2008, vol. 3, no. 1, pp. 19–23.
3. Ivanisenko, Yu., MacLaren, I., Sauvage, X., Valiev, R.Z., and Fecht, H.J., Shear-induced $\alpha \to \gamma$ transformation in nanoscale Fe-C composite, *Acta Mater.*, 2006, vol. 54, no. 6, pp. 1659–1669. https://doi.org/10.1016/J.ACTAMAT.2005.11.034
4. Seo, J.-W., Jun, H.-K., Kwon, S.-J., and Lee, D.-H., Rolling contact fatigue and wear of two different rail steels under rolling-sliding contact, *Int. J. Fatigue*, 2016, vol. 83, no. 2, pp. 184–194. https://doi.org/10.1016/J.IJFATIGUE.2015.10.012
5. Lewis, R., Christoforou, P., Wang, W.J., Beagles, A., Burstow, M., and Lewis, S.R., Investigation of the influence of rail hardness on the wear of rail and wheel materials under dry conditions (ICRI wear mapping project), *Wear*, 2019, vols. 430–431, pp. 383–392. https://doi.org/10.1016/j.wear.2019.05.030
6. Skrypnyk, R., Ekh, M., Nielsen, J.C.O., and Palsson, B.A., Prediction of plastic deformation and wear in railway crossings—Comparing the performance of two rail steel grades, *Wear*, 2019, vols. 428–429, pp. 302–314. https://doi.org/10.1016/j.wear.2019.03.019
7. Kim, D., Quagliato, L., Park, D., and Kim, N., Lifetime prediction of linear slide rails based on surface abrasion and rolling contact fatigue-induced damage, *Wear*, 2019, vols. 420–421, pp. 184–194. https://doi.org/10.1016/j.wear.2018.10.015
8. Huang, Y.B., Shi, L.B., Zhao, X.J., Cai, Z.B., Liu, Q.Y., and Wang, W.J., On the formation and damage mechanism of rolling contact fatigue surface cracks of wheel/rail under the dry condition, *Wear*, 2018, vols. 400–401, pp. 62–73. https://doi.org/10.1016/j.wear.2017.12.020
9. Gromov, V.E., Ivanov, Yu.F., Yur'ev, A.A., and Morozov, K.V., *Differentsirovanno-zakalennye rel'sy: evolyutsiya struktury i svoistv v protsesse ekspluatatsii* (Differentially Hardened Rails: Evolution of Structure and Properties during Operation), Novokuznetsk: Sib. Gos. Ind. Univ., 2017.
10. Ivanov, Yu.F., Gromov, V.E., Glezer, A.M., Peregudov, O.A., and Morozov, K.V., Nature of the structural degradation rail surfaces during operation, *Bull. Russ. Acad. Sci.: Phys.*, 2016, vol. 80, no. 12, pp. 1483–1488. https://doi.org/10.3103/S1062873816120078
11. Kormyshev, V.E., Gromov, V.E., Ivanov, Yu.F., Glezer, A.M., Yuriev, A.A., Semin, A.P., and Sundeev, R.V., Structural phase states and properties of rails after long-term operation, *Mater. Lett.*, 2020, vol. 268, art. ID 127499. https://doi.org/10.1016/j.matlet.2020.127499
12. Kormyshev, V.E., Ivanov, Yu.F., Gromov, V.E., Yur'ev, A.A., and Polevoi, E.V., Structure and properties of differentially quenched 100-m rails after an extremely long-term operation, *Fundam. Probl. Sovrem. Materialoved.*, 2019, vol. 16, no. 4, pp. 538–546. https://doi.org/10.25712/ASTU.1811-1416.2019.04.016
13. Kormyshev, V.E., Polevoi, E.V., Yur'ev, A.A., Gromov, V.E., and Ivanov, Yu.F., The structural formation in differentially-hardened 100-meter-long rails during long-term operation, *Steel Transl.*, 2020, vol. 50, no. 2, pp. 77–83. https://doi.org/10.3103/S0967091220020047
14. Kormyshev, V.E., Ivanov, Yu.F., Yur'ev, A.A., Polevoi, E.V., Gromov, V.E., and Glezer, A.M., Evolution of structural-phase states and properties of differentially hardened 100-meter rails during extremely long operation. Report 1. Structure and properties of rail steel before operation, *Probl. Chern. Metall. Materialoved.*, 2019, no. 4, pp. 50–56.
15. Kormyshev, V.E., Gromov, V.E., Ivanov, Yu.F., and Glezer, A.M., Structure of differential hardened rails under severe plastic deformation, *Deform. Razrushenie Mater.*, 2020, no. 8, pp. 16–20. https://doi.org/10.31044/1814-4632-2020-8-16-20
16. Gol'dshtein, M.I. and Farber, B.M., *Dispersionnoe uprochnenie stali* (Dispersion Hardening of Steel), Moscow: Metallurgiya, 1979.
17. Pickering, F.B., *Physical Metallurgy and the Design of Steels*, London: Applied Science, 1978.
18. Predvoditelev, A.A., Current state of research of dislocation ensembles, in *Problemy sovremennoi kristallografii* (Modern Crystallography), Moscow: Nauka, 1975, pp. 262–275.
19. Friedman, L.H. and Chrzan, D.C., Scaling theory of the hall-petch relation for multilayers, *Phys. Rev. Lett.*, 1998, vol. 81, no. 13, art. ID 2715. https://doi.org/10.1103/PhysRevLett.81.2715

20. Morito, S., Nishikawa, J., and Maki, T., Dislocation density within lath martensite in Fe-C and Fe-Ni alloys, *ISIJ Int.*, 2003, vol. 43, no. 9, pp. 1475–1477. https://doi.org/10.2355/isijinternational.43.1475

21. Kim, J.G., Enikeev, N.A., Seol, J.B., Abramova, M.M., Karavaeva, M.V., Valiev, R.Z., Park, C.G., and Kim, H.S., Superior strength and multiple strengthening mechanisms in nanocrystalline TWIP steel., *Sci. Rep.*, 2018, vol. 8, art. ID 11200. https://doi.org/10.1038/s41598-018-29632-y

22. Ganji, R.S., Karthik, P.S., Rao, K.B.S., and Rajulapati, K.V., Strengthening mechanisms in equiatomic ultrafine grained AlCoCrCuFeNi high-entropy alloy studied by micro- and nanoindentation methods, *Acta Mater.*, 2017, vol. 125, pp. 58–68. https://doi.org/10.1016/j.actamat.2016.11.046

23. Morales, E.V., Galeano Alvarez, N.J., Morales, A.M., and Bott, I.S., Precipitation kinetics and their effects on age hardening in an Fe-Mn-Si-Ti martensitic alloy, *Mater. Sci. Eng., A*, 2012, vol. 534, pp. 176–185. https://doi.org/10.1016/j.msea.2011.11.056

24. McLean, D., *Mechanical Properties of Metals*, Chichester: Wiley, 1962.

25. Embyri, I.D., Strengthening by dislocations structure, in *Strengthening Method in Crystals*, Kelly, A. and Nicholson, R.B., Eds., London: Applied Science, 1971, pp. 331–402.

26. Koneva, N.A. and Kozlov, E.V., Physical nature of the stages of plastic deformation, in *Strukturnye urovni plasticheskoi deformatsii i razrusheniya* (Structural Levels of Plastic Deformation and Destruction), Panin, V.E., Ed., Novosibirsk: Nauka, 1990, pp. 123–186.

27. Yao, M.J., Welsch, E., Ponge, D., Haghighat, S.M.H., Sandlobes, S., Choi, P., Herbig, M., Bleskov, I., Hickel, T., Lipinska-Chwalek, M., Shantraj, P., Scheu, C., Zaefferer, S., Gault, B., and Raabe, D., Strengthening and strain hardening mechanisms in a precipitation-hardened high-Mn lightweight steel, *Acta Mater.*, 2017, vol. 140, pp. 258–273. https://doi.org/10.1016/j.actamat.2017.08.049

28. Han, Y., Shi, J., Xu, L., Cao, W.Q., and Dong, H., TiC precipitation induced effect on microstructure and mechanical properties in low carbon medium manganese steel, *Mater. Sci. Eng., A*, 2011, vol. 530, pp. 643–651. https://doi.org/10.1016/j.msea.2011.10.037

29. Silva, R.A., Pinto, A.L., Kuznetsov, A., and Bott, I.S., Precipitation and grain size effects on the tensile strain-hardening exponents of an API X80 steel pipe after high-frequency hot-induction bending, *Metals*, 2018, vol. 8, no. 3, art. ID 168. https://doi.org/10.3390/met8030168

30. Morales, E.V., Gallego, J., and Kestenbachz, H.-J., On coherent carbonitride precipitation in commercial microalloyed steels, *Philos. Mag. Lett.*, 2003, vol. 83, no. 2, pp. 79–87. https://doi.org/10.1080/0950083021000056632

31. Fine, M.E. and Isheim, D., Origin of copper precipitation strengthening in steel revisited, *Scr. Mater.*, 2005, vol. 53, no. 1, pp. 115–118. https://doi.org/10.1016/j.scriptamat.2005.02.034

32. Shtremel', M.A., *Prochnost' splavov. Chast' 2. Deformatsiya* (Strength of Alloys, Part 2: Deformation), Moscow: Mosk. Inst. Stali Splavov, 1997.

33. Mott, N.F. and Nabarro, F.R.N., An attempt to estimate the degree of precipitation hardening, with a simple model, *Proc. Phys. Soc.*, 1940, vol. 52, no. 1, pp. 86–93. https://doi.org/10.1088/0959-5309/52/1/312

34. Belen'kii, B.Z., Farber, B.M., and Gol'dshtein, M.I., Estimates of strength of low-carbon low-alloy steels according to structural data, *Fiz. Met. Metalloved.*, 1975, vol. 39, no. 3, pp. 403–409.

35. Huthcinson, B., Hagström, J., Karlsson, O., Lindell, D., Tornberg, M., Lindberg, F., and Thuvander, M., Microstructures and hardness of as-quenched martensites (0.1–0.5% C), *Acta Mater.*, 2011, vol. 59, no. 14, pp. 5845–5858. https://doi.org/10.1016/j.actamat.2011.05.061

36. Senkov, O.N., Scott, J.M., Senkova, S.V., Miracle, D.B., and Woodward, C.F., Microstructure and room temperature properties of a high-entropy TaNbHfZrTi-alloy, *J. Alloys Compd.*, 2011, vol. 509, no. 20, pp. 6043–6048. https://doi.org/10.1016/j.jallcom.2011.02.171

37. Sieurin, H., Zander, J., and Sandström, R., Modeling solid solution hardening in stainless steels, *Mater. Sci. Eng., A*, 2006, vol. 415, nos. 1–2, pp. 66–71. https://doi.org/10.1016/j.msea.2005.09.031

38. Vöhringer, O. and Macherauch, E., Struktur und mechanische Eigenschaften von Martensit, *J. Heat Treat. Mater.*, 1977, vol. 32, no. 4, pp. 153–168. https://doi.org/10.1515/htm-1977-320401

39. Prnka, T., Quantitative relationships between the parameters of dispersed precipitates and the mechanical properties of steels, *Met. Sci. Heat Treat.*, 1975, vol. 17, pp. 548–552.

*Translated by S. Kuznetsov*